Search of point defect transition states in hcp twin boundaries: The monomer method

V. P. Ramunni,* M. A. Alurralde, and R. C. Pasianot†
Departamento de Materiales, CAC/CNEA, Avda. Gral. Paz 1499, 1650 San Martín, Argentina
(Received 10 November 2005; revised manuscript received 8 February 2006; published 30 August 2006)

We develop the monomer, a molecular statics technique for the search of transition states under conditions of relatively complex atomistic environments. As its counterpart from the literature, the dimer, our method is based on forces evaluation alone and is able to find the saddle configuration without previous knowledge of the equilibrium state across the saddle; at variance with it, the needed local curvature is determined with just one force evaluation per iteration step. The method is here applied to the location of saddle configurations relevant to the migration of vacancies and self-interstitials in the $(11\bar{2}1)$ and $(11\bar{2}2)$ twin boundaries of α-Zr modeled with an embedded atom type interatomic potential. Besides the fundamental interest of studying migration in these environments of reduced symmetry and dimensionality, we aim at a better understanding of grain boundaries as agents contributing to the mechanical deformation under irradiation conditions. Whereas vacancies have already been studied in the same boundaries employing a different methodology, self-interstitial results are new. For comparison purposes and completeness however, some results relating to vacancies are also included. Our main findings relate to the prediction of very low interstitial migration energies that radically change the anisotropy of bulk migration. This behavior may be associated, though not necessarily, with spatially extended configurations. The results suggest that the picture of grain boundaries as essentially perfect sinks, common to models of irradiation creep and growth, may need revision.

DOI: 10.1103/PhysRevB.74.054113 PACS number(s): 61.72.Bb, 31.15.Qg, 61.80.−x

I. INTRODUCTION

Several methods of locating transition states on the potential energy surface of a system have been proposed in the literature, mostly coming from theoretical chemistry and requiring evaluation of the second derivatives of the energy with respect to the coordinates, e.g., Ref. 1–6. Such methods become however too expensive and therefore impractical when the system possesses many degrees of freedom (say $n > 10^3$) as commonly encountered in atomistic simulations, the more so if *ab initio* quantum mechanical calculations are involved. In a pioneering work, Sinclair and Fletcher[7] advanced a method relaying only on forces, a variant of the conjugate gradients technique, and applied it to a crack model in Si possessing 500 degrees of freedom. More recently force methods have received renewed attention, being the so called nudged elastic band[8] and dimer[9] among the most popular. The former requires knowledge of the two (local) minimum energy states connected by the transition, and is more aimed at obtaining the whole minimum energy path. Such a knowledge is not required by the latter, so that it is better tailored to situations of increased structure complexity. In this sense, they can be viewed as complementary. Also, both methods are pictorially described in terms of interacting/correlated system images, the former using several of them, while the latter involves only two.

The method presently developed is inspired by the dimer one and possesses equivalent capabilities, then the given name monomer. We do not however resort to the picture of system images but to more standard mathematical reasoning. Specifically, both methods rely on finding the least local curvature of the potential energy surface, C, and from the corresponding eigenvector $\boldsymbol{v}$ define an effective force, $\boldsymbol{F}_{\text{eff}}$, able to drive the system towards a saddle configuration. Similarly to[9] we use

$$\boldsymbol{F}_{\text{eff}} = \boldsymbol{F}_0 - 2\frac{\boldsymbol{F}_0 \cdot \boldsymbol{v}}{|\boldsymbol{v}|^2}\boldsymbol{v} \quad \text{for } C < 0, \tag{1}$$

where $\boldsymbol{F}_0$ is the force at the current point $\boldsymbol{R}_0$; this amounts to reverse the force component along the curvature eigenvector while keeping unchanged all the other ones. On the other hand, for regions where $C > 0$ we use the naive approach of pulling the system uphill along the vector $-\boldsymbol{F}_0 \cdot \boldsymbol{v}\boldsymbol{v}$ (fixed) until the condition $C < 0$ is fulfilled. More details are given later on.

Our main purpose is to develop a practical technique able to locate point defect transition states, and therefore the migration barriers, in atomistic simulations of low symmetry systems, such as grain boundaries (GB), that most likely involve the coordinated motion of several atoms at a time. A particularly relevant field of application relates to the radiation present in a CANDU™ nuclear reactor that produces important deformations of the pressure tubes made of Zr alloys, via the creep and growth phenomena; chiefly axial elongation and diameter increase. These deformations are the result of the interplay between the anisotropy of the hcp crystal structure, the fabrication texture, and the irradiation-produced point defects that flow and accumulate at dislocations, loops, and GBs. Even though current models are consistent at predicting the elongation,[10–12] the diameter increase may result too small or even negative. The models identify the GBs as central to the later deformation, considering them as perfectly absorbing sinks, namely, the grain walls advance or recede according to the positive/negative contribution of each interstitial/vacancy flowing through. Interestingly, this rather passive picture somewhat contrasts with the character of diffusion short-circuit attributed to GBs, mechanism that plays an important role in high temperature metallurgical processes.[13] One may wonder then how would such a picture

be affected when the GB region is populated with potentially fast moving interstitials at the typical reactor working temperatures of 500–600 K.

The present work succinctly describes the point defect structures and their migration modes that were found by applying the monomer technique to the core region of the $(11\bar{2}1)$ and $(11\bar{2}2)$ twin boundaries in hcp α-Zr modeled with an embedded atom (EAM) type interatomic potential; we recall that twin formation is a common deformation mechanism in hexagonal metals due to the partial lack of slip systems. The same GBs were previously studied in Refs. 14 and 15 regarding vacancies but using a different, less sophisticated, technique. In Sec. II the methodology for the GB generation and the handling of point defects are described; also included are the details on the monomer procedure. Section III reports the results on defect structures and migration modes; finally Sec. IV summarizes our main conclusions.

II. SIMULATION METHODS

A. GBs and point defect generation

The Zr EAM-type interatomic potential here employed[16] is the same of previous studies on bulk and GBs properties. Relevant aspects within the present context are that it reproduces a bulk vacancy migration energy rather low but consistent with experiment,[17] about 0.6 eV, and that it predicts the basal crowdion (Bc) as the most stable interstitial configuration with very fast, even athermal[18] migration, mostly restricted to the basal planes.

The GB generation method is rather standard. Briefly, the surrounding cubic crystallite consists of some 3000 freely moving atoms limited by rigid boundaries on the z axis and periodic conditions on the (x,y) plane of the GB. Two half-crystals of chosen orientations are matched approximately at the $z=0$ coordinate, and the system is then energetically relaxed using a molecular statics procedure based on the conjugate gradients technique. The energy minimization is undertaken in two stages; in the first of them the two half-crystals are rigidly displaced relative to each other, while the second also allows individual atomic displacements (that dominate the relaxation). The procedure assures well relaxed structures with very low stresses and forces. Figure 1 shows a view perpendicular to the $[1\bar{1}00]$ axis of the two twins studied, namely $(11\bar{2}1)$ (TW1 from now on) and $(11\bar{2}2)$ (id TW2), indicating their main geometrical elements; the four different symbols show the stacking of atomic planes along $[1\bar{1}00]$. We obtain formation energies of 102 and 161 mJ/m^2 respectively, in good agreement with previous works. Symmetry operations worth noticing that aid in later analyses are the 180° rotation about the $x\equiv[11\bar{2}6]$ twinning axis for TW1, and the $(1\bar{1}00)[11\bar{2}3]/6$ mirror glide for TW2. Also, the GB plane of TW2 is a mirror plane of the structure. We note that results regarding TW2 are generally easier to describe, they are then presented before the ones pertaining to TW1.

Regarding the point defects, an interstitial/vacancy is introduced in the above GBs by addition/subtraction of an

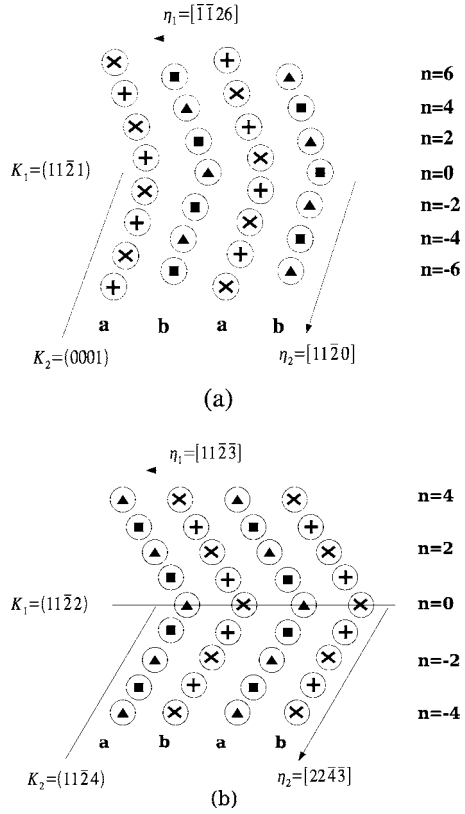

FIG. 1. Scheme of the two GBs studied showing main elements, (a) TW1 and (b) TW2.

atom at several positions followed by a new energy relaxation, obtaining so the corresponding structures and formation energies, the latter given by

$$E_f = E_{N\pm1} \mp E_c - E_N, \tag{2}$$

where E_N refers to an N-atom crystallite's energy (+1/−1 for the interstitial/vacancy), and the cohesive energy E_c compensates for the extra/missing atom. The chosen crystallite's size assures well converged energies and structures for all configurations close to the GB.

B. Transition states search

The uniqueness of the monomer method resides in the relative economy to evaluate the minimum local curvature C. As is well known, being $\boldsymbol{H}$ the Hessian matrix, the variational minimization of the Rayleigh quotient $\mathcal{R}=\boldsymbol{x}\cdot\mathbf{H}\cdot\boldsymbol{x}/|\boldsymbol{x}|^2$ obtains C, while the eigenvector $\boldsymbol{v}$ is given by the optimal $\boldsymbol{x}$. The minimization is here performed by means of the conjugate gradients technique, the needed gradient being given by $\nabla\mathcal{R}=2(\mathbf{H}-\mathcal{R})\cdot\boldsymbol{x}/|\boldsymbol{x}|^2$. Notably, $\mathbf{H}$ is never explicitly computed but only the necessary matrix element by resorting to the Taylor expansion of the energy about $\boldsymbol{R}_0$. Assuming local harmonicity, the energy and force are obtained at the nearby point $(\boldsymbol{R}_0+\Delta\boldsymbol{R})$ according to

$$E^+ \approx E_0 - \boldsymbol{F}_0\cdot\Delta\boldsymbol{R} + \tfrac{1}{2}\Delta\boldsymbol{R}\cdot\boldsymbol{H}\cdot\Delta\boldsymbol{R}, \tag{3a}$$

$$\boldsymbol{F}^{+} \approx \boldsymbol{F}_0 - \boldsymbol{H} \cdot \Delta \boldsymbol{R}, \tag{3b}$$

where $\Delta \boldsymbol{R}$ is parallel to the current $\boldsymbol{x}$ and of a small enough (fixed) size, and $\boldsymbol{F}=-\nabla E$. From Eqs. (3) $\mathcal{R}$ and $\nabla\mathcal{R}$ are easily expressed as

$$\mathcal{R} = 2(E^{+} - E_0 + \boldsymbol{F}_0 \cdot \Delta \boldsymbol{R})/|\Delta \boldsymbol{R}|^2, \tag{4a}$$

$$\nabla\mathcal{R} = 2(\boldsymbol{F}_0 - \boldsymbol{F}^{+} - \mathcal{R}\Delta \boldsymbol{R})/|\Delta \boldsymbol{R}||\boldsymbol{x}|. \tag{4b}$$

In the present context, the monomer method can be thought of as an asymmetrical formulation of the dimer one, the latter also including information from the point $(\boldsymbol{R}_0 - \Delta \boldsymbol{R})$.

In summary, operationally the system is started from a local equilibrium configuration represented by the defect. The atomic positions in some vicinity of the latter are then randomly perturbed, so defining a direction along which the system is marched until the condition $C<0$ is met. From there on Eq. (1) is used within a tailored conjugate gradient scheme, where $\boldsymbol{F}_0$ is recalculated but $\boldsymbol{v}$ is kept fixed during the line search stage that connects one configuration to the next one in the iteration process. At the beginning of each iteration step Eqs.(4) are used within another conjugate gradients scheme to update C and $\boldsymbol{v}$. Besides some security checks, the iterations end by finding a saddle configuration when all the forces get below a chosen level. Once at this point the system is perturbed along $\boldsymbol{v}$ to undertake a standard energy minimization that allows us to find the other local minimum across the saddle. Currently about 10^3 randomly selected directions are followed, and no measures are taken to avoid repetitions in order to improve efficiency. This is complemented by marching the system along few selected initial directions suggested by inspection in order to search for possibly missed saddles. Though such a naive approach leaves room for improvement, we believe it to be sufficient for the present purposes.

We shall close this section with a discussion on the potential advantages of the monomer technique as compared to the dimer one. There are two broad and fairly independent steps to consider, namely, finding the local curvature and translating the configuration. Regarding the latter we have just stated that our technique has not been tuned; it is clear however that any of the improvements discussed in Ref. 9 can be carried over to the present scheme with no significant changes. The main difference resides then in the former step. A first though somewhat subjective observation, refers to the almost trivial present derivation as compared to the one in Ref. 9; this helps programming and code maintenance. Besides, the conjugate gradients algorithm, used here to optimize the Rayleigh quotient, is a well tested technique widely available in mathematical software libraries. A second and more fundamental point refers to the economy in computational resources: The monomer reduces roughly by half the number of needed force evaluations; this represents a sizable time savings particularly in the context of *ab initio* calculations where it is a critical time-consuming step. Each rotation (iteration) of the dimer towards finding the minimum local curvature at $\boldsymbol{R}_0$ involves the computation of energy and forces at the two points $\boldsymbol{R}_0 \pm \Delta \boldsymbol{R}$; in fact, quantities at $\boldsymbol{R}_0$ are never explicitly computed but interpolated from these two points. Contrary, the present technique evaluates energy and forces only once at $\boldsymbol{R}_0$ and, with each subsequent iteration, at $\mathbf{R}_0 + \Delta \boldsymbol{R}$. An interesting final observation is that the dimer rotation methodology is very akin to Jacobi's iterative method for diagonalizing symmetrical matrices by succesive rotations within two-dimensional subspaces, see, e.g., Chap. 7 of Ref. 19. The way the rotation plane is chosen[9] basically has the effect of maximizing before rotation the absolute value of the matrix off-diagonal element within the plane, which constitutes an optimal strategy in the present context. As a test then, we have coded an asymmetrical (in the above sense) formulation of the problem along these lines and have compared it with the optimization of the Rayleigh quotient, so as to keep on equal footing the number of forces evaluations per iteration. The tests consisted in finding the smallest few eigenvalues of large numerical matrices (typically 3000×3000) and in every case the Rayleigh quotient minimization was found to be at least as efficient as the rotation method.

TABLE I. Minimum interstitial/vacancy (I/V) formation energies (in eV) for the two twin boundaries studied in α-Zr.

	TW1	TW2	Bulk
I	2.21	1.46	2.50
V	1.40	1.50	1.74

III. RESULTS

A. Minimum energy point defect structures

The results for the vacancy are similar to earlier reports,[14,15] namely, formation energies in the GB core are lower than bulk ones, the latter being approached starting at about $n=\pm 5$ in Fig. 1. The minimum energy is not obtained for $n=0$ as one might expect but for $n=\pm 1$. A slight difference with previous results is that for TW2 we obtain a delocalized vacancy with vacant sites at $n=\pm 1$ and an atom in between at $n=0$; this was reported before as a saddle configuration bridging the states at $n=\pm 1$ with a very small barrier though, 0.04 eV. No other delocalized structure was presently found. Table I reports the calculated point defect global minimum energies for the two twins.

Interstitial structure varies considerably among the twins. For TW2 it can be described as a dumbbell of varying orientation. For $n=0$ it is strictly on the GB plane and oriented at about 45° of the $[1\bar{1}00]$ atomic rows, with formation energy of 1.46 eV; for $n=1$ it is slightly below and nonparallel to the GB plane, with formation energy of 1.93 eV; for larger n it switches gradually to the bulk configuration of basal crowdion along the $[11\bar{2}0]$ rows, which is almost reached for $n=5$. Also, the mirror glide symmetry forces equivalent configurations for coordinates **a** and **b** along $[1\bar{1}00]$ rows.

On the other hand interstitial structures in TW1 show a wider variety. The minimum energy one corresponds to a single atom at an off-site position on $n=0$ close to a **b** row and intersecting the 180° rotation axis. All the remaining

configurations do possess extended nature, involving at least three off-site atoms. Generally but not exclusively, extended configurations more or less parallel to the GB plane possess energies not beyond 2.3 eV; no structure of this type was found on $n=0$ though. Other extended structures involving features perpendicular to the GB plane, may reach typical bulk values of 2.5 eV, even if centered on the GB core.

Compared to previous studies of model fcc GBs, e.g., Ref. 20, that report point defect formation energies of just a small fraction of bulk values, our results may seem too high. However, once noticing the present rather low GB energies, this is consistent with the known tendency to larger diffusion coefficients the larger the GB energy.[13] Also, simulations of vacancies in nonsymmetric GBs performed with a slightly modified version of the present Zr potential[15] report fairly lower vacancy energies (0.3–0.5 eV) for GBs of sizeable larger energy (400–500 mJ/m^2). Extended equilibrium interstitial configurations do not seem to be a common finding, however they have been reported before in studies of diffusion in model Cu twist boundaries,[21] and are clearly not beyond expectations. On one side even in crystalline environments there are migration mechanisms involving coordinated atomic motion, e.g., the interstitialcy one. On the other, TW1 presents a rather compact structure without obvious open spaces able to fit extra atoms, therefore the enhanced relaxations entailed by an extended structure would tend to lower the formation energy.

B. Transition states

For the location of transition states we select the above minimum energy point defect structures and apply the monomer procedure already outlined. The several resulting saddle configurations are subjected to energy relaxation along the two senses of the jumping eigenvector, then assuring the pertinence of the saddle to the starting configuration and also locating the new minimum across it. These minima are in turn new starting configurations where from the searching procedure is started again, and so on. The search is restricted to configurations pertaining to the GB core and with saddle energies (i.e., activation energies) up to about bulk values. Also for both, vacancies and interstitials, most jumps that can be derived from the ones reported in the following, e.g., reverse jumps and those equivalent by symmetry, are not explicitly included.

Regarding vacancies, but for small numerical differences the results generally agree with previous works,[14,15] that force the jumping eigenvector to be fixed and parallel with the difference vector between final and initial configuration. On the other hand, vacancy calculations are here performed mainly as a consistency check for the present technique. In view of this we only present results for TW2 because they are easier to describe and show some minor, hardly essential, differences with the previous reports. Table II summarizes the results for the vacancy in TW2, the associated configurations being depicted in Fig. 2. The first column details the jump, E_m is the corresponding migration barrier, E_f is the formation energy of the final configuration, and E_{sp} is the saddle point energy; numbers within parenthesis label the jumps shown in the figure. We have found it clearer to depict the configurations using the unrelaxed GB structure, the figure then respects symmetry elements but distances are quite off scale, particularly, consecutive atoms along $[1\bar{1}00]$ rows appear too close to each other. Relevant jump barriers for long range migration start at about 0.3 eV, compared to the bulk 0.6 eV, and most jumps occur between close neighbors. Transition (**6**) is an instance of a double jump not reported before, the associated barrier though is rather high; also of note is the present jump (**1**) involving the delocalized $\mathbf{V}_{1,-1}$ vacancy. When considering however the reverse jump taking only 0.01 eV (cf. Table II) it is perhaps more appropriate to think of it as a flat barrier. A flat barrier is also found for jump (**2**) though the minimum at the top of it is very shallow and therefore was not included in the table.

TABLE II. Vacancy jumps in the TW2 boundary. Migration, formation, and saddle point energies (E_m,E_f,E_{sp}) in eV. The first column refers to the jumps depicted in Fig. 2. See main text for more details.

Transition		E_m	E_f	E_{sp}
$\mathbf{V_1}\rightarrow\mathbf{V_{1,-1}}$	(**1**)	0.058	1.538	1.548
$\mathbf{V_0}\rightarrow\mathbf{V_{0'}}$	(**2**)	0.279	1.731	2.010
$\mathbf{V_1}\rightarrow\mathbf{V_{1'}}$	(**3**)	0.313	1.495	1.803
$\mathbf{V_1}\rightarrow\mathbf{V_0}$	(**4**)	0.638	1.731	2.128
$\mathbf{V_{-1}}\rightarrow\mathbf{V_0}$	(**5**)	0.883	1.738	2.378
$\mathbf{V_0}\rightarrow\mathbf{V_{1'}}$	(**6**)	0.989	1.491	2.719

As expected from the structure analysis, interstitial migration mechanisms are very different among the two boundaries, therefore they are treated separately in what follows. Table III gathers the results for TW2, the associated configurations being shown in Fig. 3. $\mathbf{A}_n$ and $\mathbf{B}_n$ refer to dumbbells on plane n related through the mirror glide symmetry, different positions on the same plane are denoted with numerical superscripts. The search process was started from $\mathbf{A}_0$ in Fig. 3, the dotted/full arrows conveying an idea of the replacement sequence for the first/second search stage. Jumps are mostly shown as initiated by one member of the dumbbell, though of course there are the symmetrical ones started by the other member, an example of this is the transition $\mathbf{A_0}\rightarrow\mathbf{B_0}$ with respect to $\mathbf{A_0}\rightarrow\mathbf{B_0^3}$. A more obvious example of symmetry related transitions are $\mathbf{A_0}\rightarrow\mathbf{A_1}$ with $\mathbf{B_0}\rightarrow\mathbf{B_1^1}$.

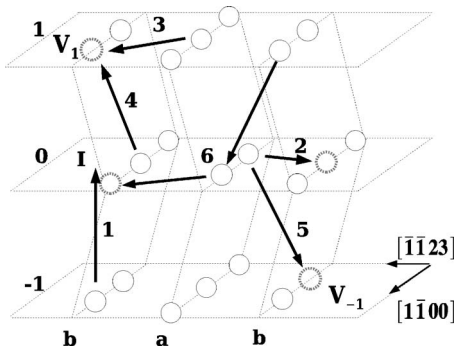

FIG. 2. Vacancy jumps in the TW2 boundary.

TABLE III. Interstitial jumps in the TW2 boundary. Migration, formation, and saddle point energies (E_m, E_f, E_{sp}) in eV. The first column refers to the jumps depicted in Fig. 3.

Transition	E_m	E_f	E_{sp}
$\mathbf{A_0}\rightarrow\mathbf{B_0}$	0.042	1.458	1.500
$\mathbf{A_0}\rightarrow\mathbf{B_0^3}$	0.043	1.457	1.500
$\mathbf{A_0}\rightarrow\mathbf{A_1}$	0.483	1.930	1.942
$\mathbf{A_0}\rightarrow\mathbf{B_1}$	0.491	1.930	1.951
$\mathbf{A_0}\rightarrow\mathbf{A_0^1}$	0.828	1.458	2.288
$\mathbf{B_0}\rightarrow\mathbf{B_1^1}$	0.485	1.930	1.943
$\mathbf{A_1}\rightarrow\mathbf{B_0^2}$	0.021	1.457	1.951
$\mathbf{A_0^1}\rightarrow\mathbf{B_0^1}$	0.988	1.457	2.446
$\mathbf{B_0}\rightarrow$bulk	1.047	2.479	2.505

Mainly close neighbor sites are involved in the jumps, longer range ones requiring higher activation energies; transition $\mathbf{A_0}\rightarrow\mathbf{A_0^1}$ is a notable instance of this with the participation of an atom on $n=-1$ and the final dumbbell on the starting $n=0$ plane. Close neighbors jumps may also take place via alternative saddles; clearly $\mathbf{A_0}\rightarrow\mathbf{B_0^3}$ and $\mathbf{A_0^1}\rightarrow\mathbf{B_0^1}$ possess equivalent starting and final configurations, however the barrier for the first one, essentially a continuous slide of one dumbbell member towards a lattice site, is much lower than for the second one, requiring dumbbell on-site rotation and therefore the opening of atoms of the **b** rows on $n=\pm1$. Contrary to what the jump $\mathbf{A_0}\rightarrow\mathbf{B_0^3}$ may suggest, transitions of the type $\mathbf{A_1}\rightarrow\mathbf{B_1}$ seem very unlikely; this is however consistent with the small barrier for $\mathbf{A_1}\rightarrow\mathbf{B_0^2}$ (and for $\mathbf{A_0}\leftarrow\mathbf{A_1}$, $\mathbf{A_0}\leftarrow\mathbf{B_1}$ etc.) and the fact that metastable configurations on $n=1,2$ were very difficult to obtain with the methods of Sec. II A. Related to this, the "bulk" configuration of the jump $\mathbf{B_0}\rightarrow$bulk consists of a dumbbell on a rather farther $n=4$ plane at a small angle with the basal plane corresponding to an **a** coordinate. From the standpoint of the overall interstitial migration in this boundary, the most remarkable finding is the presence of a fast one-dimensional path along the twinning direction represented by $\mathbf{B_0}\rightarrow\mathbf{A_0}\rightarrow\mathbf{B_0^3}\ldots$; two-dimensional motion such as initiated by $\mathbf{A_0}\rightarrow\mathbf{A_1}\rightarrow\mathbf{B_0^2}\ldots$ cannot be ruled out, but requires fairly higher activation energies. This result strongly contrasts with migration in the bulk, that takes place mostly on basal planes, i.e., at fixed **a**/**b** coordinates.

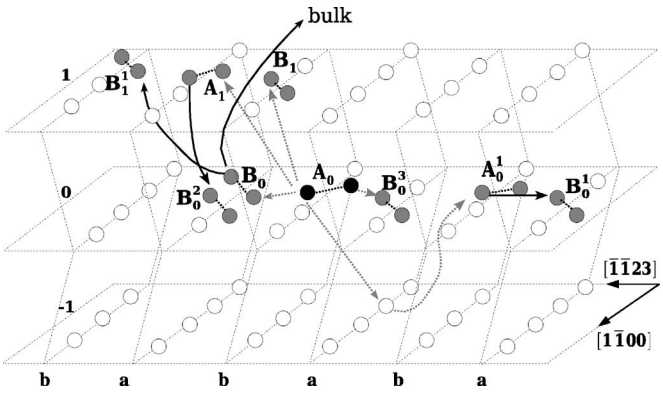

FIG. 3. Interstitial jumps in the TW2 boundary.

TABLE IV. Interstitial jumps in the TW1 boundary. Migration, formation, and saddle point energies (E_m, E_f, E_{sp}) in eV. The first column refers to the jumps depicted in Fig. 4.

Transition	E_m	E_f	E_{sp}
$\mathbf{I_0}\rightarrow\mathbf{I_1}$	0.101	2.279	2.310
$\mathbf{I_0}\rightarrow\mathbf{I_2}$	0.062	2.271	2.313
$\mathbf{I_0}\rightarrow\mathbf{I_3}$	0.279	2.281	2.489
$\mathbf{I_0}\rightarrow\mathbf{I_4}$	0.308	2.515	2.517
$\mathbf{I_0}\rightarrow\mathbf{I_5}$	0.382	2.524	2.591
$\mathbf{I_2}\rightarrow\mathbf{I_{2a}}$	0.045	2.291	2.316
$\mathbf{I_2}\rightarrow\mathbf{I_{2b}}\equiv\mathbf{I_1}$	0.058	2.279	2.329
$\mathbf{I_2}\rightarrow\mathbf{I_{2c}}$	0.159	2.299	2.430
$\mathbf{I_2}\rightarrow\mathbf{I_{2d}}$	0.198	2.285	2.469
$\mathbf{I_3}\rightarrow\mathbf{I_{3a}}$	0.022	2.301	2.303
$\mathbf{I_3}\rightarrow\mathbf{I_{3b}}\equiv\mathbf{I_{2d}^-}$	0.054	2.284	2.335
$\mathbf{I_3}\rightarrow\mathbf{I_{3c}}$	0.250	2.530	2.531
$\mathbf{I_3}\rightarrow\mathbf{I_{3d}}\equiv\mathbf{I_{2d}^-}$	0.261	2.284	2.542
$\mathbf{I_3}\rightarrow\mathbf{I_{3e}}\equiv\mathbf{I_{2c}}$	0.303	2.300	2.584
$\mathbf{I_3}\rightarrow\mathbf{I_{3f}}\equiv\mathbf{I_5}$	0.314	2.523	2.595
$\mathbf{I_3}\rightarrow\mathbf{I_{3g}}$	0.335	2.389	2.616
$\mathbf{I_3}\rightarrow\mathbf{I_{3h}}$	0.383	2.455	2.664
$\mathbf{I_4}\rightarrow\mathbf{I_{4a}}\equiv\mathbf{I_0}$	0.011	2.209	2.526
$\mathbf{I_5}\rightarrow\mathbf{I_{5a}}\equiv\mathbf{I_3^-}$	0.002	2.277	2.526
$\mathbf{I_5}\rightarrow\mathbf{I_{5b}}\equiv\mathbf{I_3}$	0.018	2.279	2.542
$\mathbf{I_5}\rightarrow\mathbf{I_{5c}}\equiv\mathbf{I_{2d}}$	0.055	2.284	2.579

Table IV and Fig. 4 summarize the results for the TW1 boundary. $\mathbf{I}_0$ was taken here as the starting configuration, leading to five different configurations identified as $\mathbf{I}_1$ to $\mathbf{I}_5$; in turn each of these were taken as new starting configurations leading to others identified now with letters, e.g., $\mathbf{I}_{2a}\ldots\mathbf{I}_{2d}$ all derive from $\mathbf{I}_2$; also, within each series the jumps are ordered according to increasing migration energy. Two stages in the search tree were thus completed and already at this level some configurations of different parent coincide or are equivalent by the 180° rotation (noted as $\mathbf{I}_x$ and $\mathbf{I}_x^-$), situation indicated by the symbol $\equiv$. Regarding Fig. 4 only a subset of the table most relevant to the discussion is shown; as before, the arrows trace the displacement sequences, when both full and dotted ones appear they stand for the first and second search stages respectively. Small black dots locate starting configurations, whereas normal size shaded circles locate the final ones; both are also tied to numbers, unprimed and primed respectively; some fine dotted lines joining atoms are drawn as an aid to the description that follows. Not unexpectedly the migration mechanisms are fairly more complex than for TW2, though some qualitative features can be extracted. Several configurations reported as local minima should in fact be considered as pertaining to the structure of nonsmooth/shallow barriers, as evidenced by their very small barrier to decay. This is the case of $\mathbf{I_4}$ in the jump $\mathbf{I_0}\rightarrow\mathbf{I_4}$ as results after comparison of its E_f with E_{sp}, the meaningful jump would then be $\mathbf{I_0}\rightarrow\mathbf{I_4}$

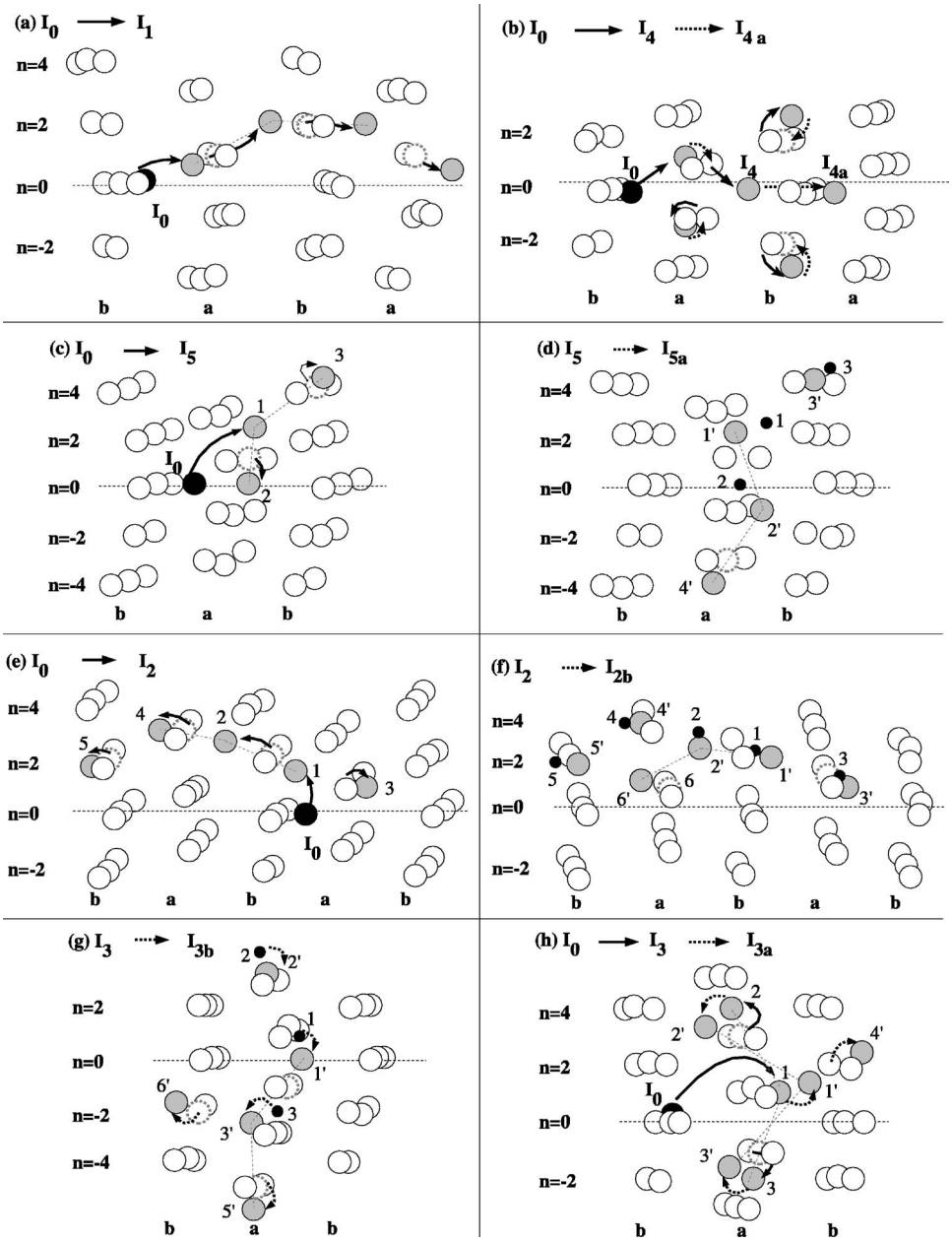

FIG. 4. Interstitial jumps in the TW1 boundary.

$\rightarrow \mathbf{I}_{4a} \equiv \mathbf{I}_{0'}$ that can also be grasped from Fig. 4(b). A similar reasoning applies to $\mathbf{I}_{3a}$ and $\mathbf{I}_{3c}$ of the $\mathbf{I}_3$ series, though we did not follow the decay events these would most probably involve features perpendicular to the GB plane, as suggested e.g., by Fig. 4(h). Another interesting example of this kind is $\mathbf{I}_5$, the jump $\mathbf{I}_0 \rightarrow \mathbf{I}_5$ suggests it to be a stable configuration, however it decays very easily according to $\mathbf{I}_5 \rightarrow \mathbf{I}_{5a} \equiv \mathbf{I}_3^-$, cf. Table IV and Figs. 4(c) and 4(d); the meaningful jump is then $\mathbf{I}_0 \rightarrow \mathbf{I}_3^-$. The series starting with $\mathbf{I}_2$ can be qualitatively described as the different configurations taken by a rather rigid string depending on the positions of its end atoms 3 and 5, Fig. 4(e). Interestingly, after noting the relative position of $\mathbf{I}_0$ with respect to $\mathbf{I}_1$ and $\mathbf{I}_2$, an easy long range migration path for $\mathbf{I}_0$ is here unraveled, namely $\mathbf{I}_0 \rightarrow \mathbf{I}_2 \rightarrow \mathbf{I}_{2b} \equiv \mathbf{I}_1 \rightarrow \mathbf{I}_{0'}$, Figs. 4(e), 4(f), and 4(a), with respective barriers of 0.06, 0.06, and 0.03 eV. This entails two-dimensional migration because the two equivalent sites **0** and **0′** on consecutive **b** rows are at different heights on the $[1\bar{1}00]$ axis and sit on the 180° rotation axis parallel with $[11\bar{2}6]$. The $\mathbf{I}_3$ series, that shares several configurations with the previous one, suggests early stages of jumps connecting to the bulk, the only exception being $\mathbf{I}_3 \rightarrow \mathbf{I}_{3e} \equiv \mathbf{I}_{2c}$ (not shown). Most jumps to the bulk preserve the basal plane (i.e. the **a** coordinate) of the starting $\mathbf{I}_3$, performing a kind of zigzag motion that can even cross the $n=0$ plane, the easiest being $\mathbf{I}_3 \rightarrow \mathbf{I}_{3b} \equiv \mathbf{I}_{2d}^-$ with a barrier of 0.05 eV, Fig. 4(g).

IV. CONCLUSIONS

We have developed and demonstrated the soundness of a technique, the monomer, as a tool able to locate transition states on potential energy surfaces, particularly in situations of relatively complex structure. Its economy in computa-

tional resources and reliance on the well tested conjugate gradients algorithm, make it an appealing technique to consider even in fields other than the present one of the atomistic simulations. The application has been here to the point defect migration mechanisms in some grain boundaries of a model hcp metal. We believe however that, as its counterpart the dimer, the technique is not limited to the relatively localized transition states studied, but that it can be applied to more extended situations such as those pertinent to dislocation glide, though this may require special and more careful handling of the initial configuration. We've seen particularly in one of the grain boundaries, TW1, that the interstitial structure can be rather complicated and that the energy barriers connecting two local minima may not look as well defined mathematical saddles but possess some structural features. Also, in several instances transition states are more related to local atomic rearrangements than to long range migration. These observations must be taken care of at the moment of using calculations of this kind to build models of diffusion, such us by means of the kinetic Monte Carlo technique, because they imply violations to strict transition state theory.[22]

We have also demonstrated that both vacancies and interstitials can be relatively mobile species within grain boundaries, and that the latter may do so at a much faster pace. More systematic studies are clearly needed to asses the validity conditions of such a statement, however it is already questioning the picture of models that envisage grain boundaries as closed surface sinks that change shape according to the count of the irradiation produced point defects that reach it. The consequences that such an inner grain boundary structure may have on growth in particular, are a matter under investigation.

ACKNOWLEDGMENT

This work has been partially supported by ANPCyT through PICT 1206164.

*Electronic address: vpram@cnea.gov.ar
†Also with Consejo Nacional de Investigaciones Científicas y Técnicas, CONICET.

[1] C. J. Cerjan and W. H. Miller, J. Chem. Phys. **75**, 2800 (1981).
[2] E. J. Savino and A. M. Monti, Phys. Status Solidi B **121**, 513 (1984).
[3] A. Banerjee, N. Adams, J. Simons, and R. Shepard, J. Phys. Chem. **89**, 52 (1985).
[4] J. Baker, J. Comput. Chem. **7**, 385 (1986).
[5] J. Nichols, H. Taylor, P. Schmidt, and J. Simons, J. Chem. Phys. **92**, 340 (1990).
[6] D. J. Wales, J. Chem. Phys. **101**, 3750 (1994).
[7] J. E. Sinclair and R. Fletcher, J. Phys. C **7**, 864 (1974).
[8] H. Jónsson, G. Mills, and K. Jacobsen, in *Classical and Quantum Dynamics in Condensed Phase Simulations*, edited by B. Berne, G. Ciccotti, and D. Coker (World Scientific, Singapore, 1998), pp. 385–404.
[9] G. Henkelman and H. Jónsson, J. Chem. Phys. **111**, 7010 (1999).
[10] W. Alexander, V. Fidleris, and R. A. Holt, in *Zirconium in the Nuclear Industry* (1976), Vol. 633 of *ASTM STP*, p. 344.
[11] R. A. Holt and E. F. Ibrahim, Acta Metall. **27**, 1319 (1979).
[12] J. R. Fernández, A. M. Monti, A. Sarce, and N. Smetniansky-De Grande, J. Nucl. Mater. **210**, 282 (1994).
[13] I. Kaur, Y. Mishin, and W. Gust, *Fundamentals of Grain and Interface Boundary Diffusion* (Wiley, Chichester, West Sussex, 1995).
[14] J. R. Fernández, A. M. Monti, R. C. Pasianot, and V. Vitek, Philos. Mag. A **80**, 1349 (2000).
[15] J. R. Fernández, A. M. Montin, and R. C. Pasianot, Metall. Mater. Trans. A **33A**, 791 (2002).
[16] R. C. Pasianot and A. M. Monti, J. Nucl. Mater. **264**, 198 (1999).
[17] G. M. Hood, R. J. Schultz, and J. A. Jackman, J. Nucl. Mater. **126**, 79 (1984).
[18] R. C. Pasianot, A. M. Monti, G. Simonelli, and E. J. Savino, J. Nucl. Mater. **276**, 230 (2000).
[19] A. S. Householder, *The Theory of Matrices in Numerical Analysis* (Dover, New York, 1975), 1st edition.
[20] M. R. Sørensen, Y. Mishin, and A. F. Voter, Phys. Rev. B **62**, 3658 (2000).
[21] M. Nomura and J. B. Adams, J. Mater. Res. **10**, 2916 (1995).
[22] G. H. Vineyard, J. Phys. Chem. Solids **3**, 121 (1957).